THE EFFECT OF MAINSTREAM TURBULENCE ON TURBINE BLADE PLATFORM COOLING WITH SIMULATED SWIRL PURGE FLOW

A Thesis

by

JIYEON LEE

Submitted to the Office of Graduate and Professional Studies of
Texas A&M University
in partial fulfillment of the requirements for the degree of

MASTER OF SCIENCE

Chair of Committee,	Je-Chin Han
Committee Members,	Sai Lau
	Hanm-Ching Chen
Head of Department,	Andreas Polycarpou

December 2015

Major Subject: Mechanical Engineering

ABSTRACT

An experimental investigation to measure the effect of mainstream turbulence on blade platform cooling effectiveness within a linear cascade has been completed. Turbulence grids generate the wide ranges of turbulence intensity, from 0.72% to 13%. To simulate the rotating condition of engine blades, velocity triangle analogy has been adopted. Different size of inclined injection hole plates produces swirl motion of purge flow, which makes three different swirl ratios of 0.4, 0.6 and 1.0. Pressure sensitive paint (PSP) technique is used to obtain detailed film cooling distribution on blade platform. The inlet Reynolds number is 250,000, and coolant to mainstream flow rate (MFR) is 1.0%. By using CO_2 as a foreign gas, density ratio 1.5 is obtained. Results show the existence of pressure gradient between suction side and pressure side. Horseshoe vortex and passage vortex sweep coolant remarkably, which results in poor film cooling coverage on the blade. Furthermore, the strength of the two vortexes increases for higher rotating conditions. However, more coolant can cover the platform by increasing turbulence intensity because turbulence can reduce the strength of vortex. Especially, film cooling effectiveness increases significantly when turbulence intensity increases from 0.72% to 3.1%.

ACKNOWLEDGEMENTS

I would like to thank my committee chair, Dr. Han, and my committee members, Dr. Lau and Dr. Chen, for their guidance, support and their time throughout the course of this research. Special thanks to Dr. Han for his dedication to teach and guide me for two years.

Thanks also go to my friends and colleagues at Gas Turbine Heat Transfer Lab for making my time at Texas A&M University a great experience. I also want to extend my gratitude to the Solar Turbines, Inc., which sponsored this project, and especially to Dr. Moon and Dr. Zhang who are my great mentors over the years.

I also thank Kevin for his love and effort to encourage me.

Finally, thanks to my mother for her encouragement, endless love and support.

NOMENCLATURE

Cax	Axial chord length
D	Hole diameter
d	Bar width of grid
s	Distance from turbulence grid to cascade inlet
I	PSP emission intensity
MFR	Coolant to mainstream mass flow rate
P	Static pressure
P_e/D	Coolant hole spacing
SR	Swirl Ratio
Tu	Mainstream turbulence intensity
V1	Blade inlet velocity
V_c	Coolant velocity
V_r	Relative velocity
W_{air}	Molecular weight of air
W_{fg}	Molecular weight of foreign gas
x	Direction along axial chord length
y	Direction along axial blade pitch
η_p	Pitchwise averaged effectiveness
θ	Coolant injection angle degree
PSP	Pressure Sensitive Paint

TABLE OF CONTENTS

Page

Page

LIST OF FIGURES

LIST OF TABLES

1. INTRODUCTION AND LITERATURE REVIEW

As result of continuous efforts to increase gas turbines efficiency and power production, the mainstream temperature that enters the turbine blade stage has been rising continuously up to 1400˚c. Since the inlet temperature is already over the yielding point of the turbine blades (1090˚c), coolant gas (980˚c) is extracted from the compressor stage and supplied through the turbine blades to protect the surface from the hot gas-a process called “film cooling.”- Because, the amount of the coolant is limited, maximizing the film cooling effect has been a main issue among gas turbine researchers. Han organized the important findings of fundamental gas turbine heat transfer [1]. Even though there are abundant literatures that cover the coolant behavior in the turbine blade platform and nozzle endwall, it is still challenging to get a clear picture of the behavior because it is significantly influenced by two types of secondary flow; Horseshoe vortex and passage vortex. They make the flow development and distribution three dimensional and complicated near nozzle endwall and blade platform. The secondary flow in the blade passage was visualized and documented by Langston [2,3] and Wang et al [4]. Horseshoe vortex and passage vortex are mainly caused by the pressure gradient between suction and pressure side. The pressure side leg horseshoe vortex develops into a much larger passage vortex as it migrates from the blade leading edge to the suction side of the neighboring blade. Several small-scale corner vortices are also created near the intersection of the blade surface and the platform. Therefore, effectively cooling down

the nozzle endwall or blade platform area has been another critical issue, so there are numerous efforts to study the coolant behavior and film cooling effectiveness on those areas. Wright et al [5] demonstrated the critical findings of the blade platform cooling technology. The vortex develops mainly due to strong pressure gradient between pressure side and suction side, which results the higher heat transfer across passage. Furthermore, increased mainstream turbulence also causes higher heat transfer. Harasgama and Burton [6], Friedrichs et al [7], Jabbari et al [8], Liu et al [9], Granser and Schulenberg [10], Roy et al [11], Lapworth et al [12], Oke and Simon [13], Colban et al [14], Kost and Nicklas [15], Nicklas [16], Zhang and Jaiswal [17] and Zhang and Moon [18] performed film cooling studies by leakage flow upfront of the nozzle endwall and found that the effectiveness is insignificant because the coolant tends to be swept away by the endwall passage vortex. Intentionally designed film cooling in front of endwall [13 and 17] also had same trend, unless a large mass flow and high cooling momentum were provided. To improve the film cooling effectiveness and to some degree survive the secondary flows near the endwall, Zhang and Moon [18, 19, 20], Burd and Simon [21], Burd at el [22], Oke at el [23] further studied the effect of velocity ratio and endwall contouring on nozzle endwall inlet film cooling. There is a noticeable improvement by increasing the velocity ratio or the contouring of the endwall, but it is not significant enough to reduce the cooling mass flow requirement. Zhang et al [24] compared the heat transfer distribution on the blade platform with three different platform profiles, shark-nose, dolphin-nose and flat-nose, and suggested shark and

dolphin nose platforms have lower heat transfer coefficient and suppressed secondary flow feature.

Particularly, the nozzle endwall and blade platform areas are directly exposed to the hot mainstream gas, therefore "purge flow cooling" has been adopted to supply additionally cooling source and prevent hot gas ingestion. Purge flow comes from the gap between the stator and the rotor for the platform cooling; likewise, leakage flow comes out from a gap between combustor exit and nozzle inlet for the nozzle endwall. Several researchers tried to examine the effect of secondary flow on purge flow and blade platform film cooling effectiveness. Gao et al [25] simulated purge flow with typical labyrinthlike seal upstream blade platform and the passage vortex was generated by delta wing. The results showed that film cooling effectiveness on the blade platform was reduced by the passage vortex. Wright et al [26] studied the combined effect of passage vortex by using delta wings and unsteady wake by using upstream stationary rods on purge flow cooling effectiveness. Wright et al [27] expanded the purge flow cooling study with film coolant from discrete holes on downstream half of the blade. The common results from two studies indicated that purge cooling was swept by passage vortex, which resulted in significantly poor film cooling coverage on the blade platform, especially on pressure side. However, they also showed that the higher mainstream turbulence (13%) could reduce the passage vortex, which brought higher film cooling effectiveness in the downstream than that in the lower turbulence intensity case (0.72%). In order to compensate the cooling coverage that is swept by passage vortex, discrete film cooling holes on the platform are commonly used. Those studies are valuable to see

the effect of passage vortex on the purge flow cooling, however, those were conducted in a stationary cascade due to difficulty to produce the complex pattern of flow that is made in a rotating condition. As a result, there have been rare efforts to simulate the purge flow in a rotating condition. Suryanarayanan et al. [28] studied film cooling effectiveness of the upstream purge flow on the blade platform with three different rotating speeds. Results showed that purge flow didn't provide sufficient film protection on the downstream region along the pressure surface because of passage vortex, and this negative effect was significant in higher rotating speed. Schobeiri et al [29] measured the impact of purge cooling on contoured endwall experimentally and numerically in rotating condition as well. Significant reduction in secondary flow on the contoured endwall was found due to the decreased pressure gradient and weakened horseshoe vortex.

In a real gas turbine, purge flow has swirl motion because the rotating blades induces tangential velocity component of coolant while the disk cavity is stationary. However, the exact swirl motion on the blade platform is unknown; hence, the size and strength of the swirl motion are also unknown. There are some studies [30,31,32] that simulated the swirl motion of purge flow in the stationary cascade using relative motion between rotor and coolant. Barigozzi et al [30] produced rotating effect using coolant injection fins with different angles (-10°, 0°, 10°), and found out the negative injection angle (considering rotating condition) enhanced passage vortex, which resulted in lower thermal protection on blade platform. Stinson et al [31] used three inclined angles (0°, 30°, 60°) to produce the different levels of rotating effect for the leakage flow on endwall

purge cooling. As the angle was directed to tangential direction (60°), the cooling coverage became significantly worse because of less axial penetration through the passage. Li et al [32] considered the wide range of swirl ratio (0.4, 0.6, 0.8,1.0) and compared the results on blade platform and suction surface. Those studies showed that the rotation effect resulted in a lower film cooling performance; consequently, neglecting the tangential force of coolant induced by rotating would be an overestimation of film cooling effectiveness.

Furthermore, transformation of coolant movement caused by turbulence makes much harder to predict the coolant distribution. The mainstream turbulence level in the gas turbine ranges from 7% to 20%, and the first-stage vane is directly exposed to highest turbulence. As seen in the studies from Jumper et al [33] and Radomsky et al [34, 35], high turbulence induced faster mixing between mainstream and coolant, which resulted in coolant dispersion in downstream region. Heat transfer augmentation was observed in the mid-path region on the endwall due to mainstream turbulence enhanced the coolant mixing. Those studies indicated that the augmentation level due to mainstream turbulence were similar between high (19.5%) and low (0.6%) turbulence cases near leading edge, where horseshoe vortex is dominant, and the suction side, where passage vortex is dominant. In other words, vortex is more dominant than the turbulence in leading edge and suction side area. Zhang et al [36] founded augmented heat transfer coefficient on the turbines blade surface with higher mainstream turbulence intensity (17%). However, several studies proved that higher mainstream turbulence could improve film cooling effectiveness. Liu et al [37] showed that more purge flow coolant

spread out near the blade platform leading edge for high turbulence case. Kadotani and Goldstein [38, 39] also showed that higher turbulence intensity is beneficial to film cooling effectiveness with higher blowing ratio. This is because larger momentum of coolant could penetrate mainstream with less influence by turbulence; furthermore, coolant was less likely disturbed by vortex formation. The results from Bon et al [40] also agreed with increased film cooling effectiveness with high turbulence at high blowing ratio because turbulence deterred coolant blow-off or diffusion in lateral region. Moreover, high turbulence increased film cooling effectiveness significantly in the mid-line region of injection holes because turbulence helped faster creation of uniform coolant between cooling jets. The study from Gregory-Smith and Cleak [41] explained the interaction between the inlet turbulent flow and secondary flow. Higher mainstream turbulence induced earlier transition near the suction surface, so it made thinner inlet boundary layer, which produced smaller vortex closer to endwall. That is, higher mainstream turbulence didn't have a direct effect on the secondary loss, but it had more effect on secondary kinetic energy, which causes more rapid dissipation of secondary flow. F. E. Ames et al [42] observed that high turbulence was not significantly affected by secondary flow on the endwall. Li et al [43] conducted experimental work recently to examine the influence of mainstream turbulence and swirl purge flow on blade platform and suction surface, and showed the higher film cooling effectiveness as increasing turbulence intensity

The efforts to investigate the sophisticated endwall/ platform region have been covered by numerous studies, however, considering the rotating effect is hard to find. As

a result, experimental results without considering rotating effect brought overestimation of cooling effectiveness.

The objective of current study is to measure the effect of mainstream turbulence and swirl purge flow on blade platform film cooling effectiveness. Wide range of mainstream turbulence intensity from 0.72% to 13% was created in upstream. Besides, inclined coolant injection hole plates and nozzle endwall trailing edge were designed to simulate the swirl motion of purge flow in order to produce relative motion in rotating condition. The obtained film cooling effectiveness distributions are expected to demonstrate the combined effect of mainstream turbulence and swirl purge flow on the rotating blade platform.

2. EXPERIMENTAL DETAILS

Current study is designed to investigate the combined effect of mainstream turbulence and swirl purge flow on blade platform across a various range of turbulence intensities and swirl ratio of purge flow. Coolant to mainstream mass flow rate (MFR) was 1.0 %. The turbulence intensity was varying from 0.72% to 13% and swirl ratio was 0.4, 0.6 and 1.0. The two extreme cases of swirl ratio 0.4 and 1.0 were examined for the previous study [43], however, the in-between swirl ratio 0.6 is considered valuable in order to complete the turbulence effect and swirl ratio study. Table 1 shows the specifications of the tested cases.

Table 1 Details of test matrix and parameters

Case #	Swirl Ratio	Injection Angle	VR*	VR**	Hole Diameter D (cm)	Hole Spacing (P/D)	Turbulence Intensity
A (Extreme Rotating)	0.4	30°	0.87	0.99	0.63	2.65	0.72% (No Grid)
B (Moderate Rotating)	0.6	45°	0.57	0.80	0.71	2.46	3.1%, 6%, 8.2% (Fine Grid)
C (Non-Rotating)	1.0	90°	0	0.40	1.00	1.87	13% (Coarse Grid)

CO_2 is used to acquire the density ratio 1.5. Experiments are conducted in a low speed wind tunnel with five cascades. Pressure Sensitive Paint (PSP) method, the mass transfer technique, has been selected to have high resolution of film cooling effectiveness distribution on blade platform without conduction loss.

2.1 Low Speed Wind Tunnel Cascade

Figure 1 shows the low speed wind tunnel facility that was designed for current study. Blades were scaled up by factor of 7.27 from Solar Turbines T-65 stage one engine blade. Figure 2 shows top view of wind tunnel and blade details of blade inlet, exit and turning angles and the blade pitch, which are 40°, 70°, 110° and 22.6cm correspondingly. Three blades are placed in the middle of passage and the thin guide blades are placed at each side border of the wind tunnel. The inlet velocity (V1) is maintained to 14m/s, and this gives mainstream Reynolds number of $2.5x10^5$ based on the blade chord length and the V1. Figure 3 shows two types of turbulence grid that were used to generate four different levels of turbulence intensity (3.1%, 6%, 8.2%, 13%). Coarse grid and fine grid were made of square bars and placed into upstream in parallel to the blade leading edge at three different distances, and Tu=0.72% was created without a grid condition. Table 2 shows the relation between the turbulence intensity and grid location, which was determined by Zhang et al. [36].

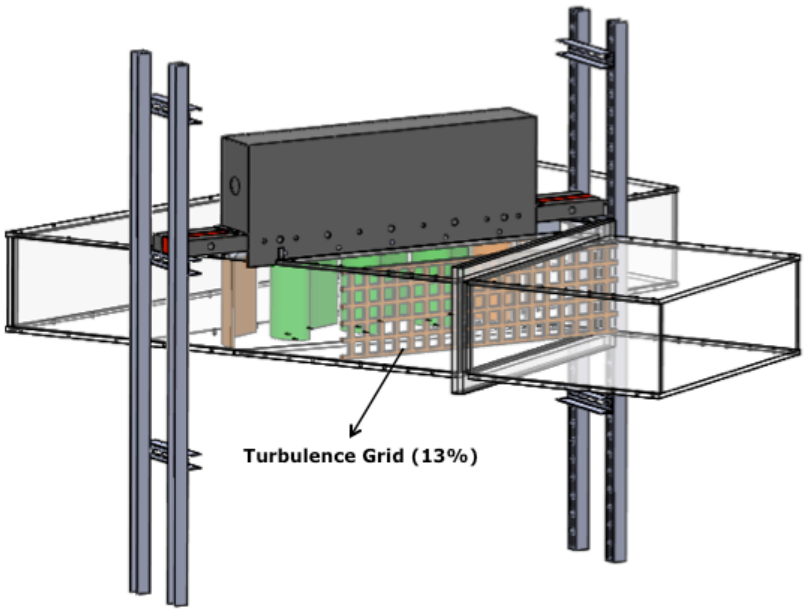

Figure 1 Low speed wind tunnel facility

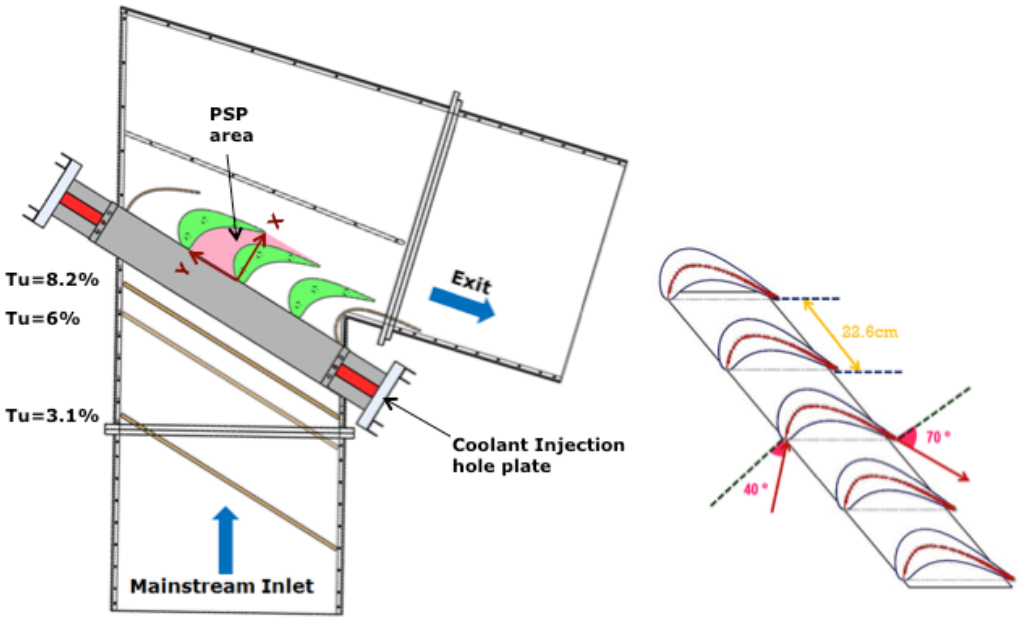

Figure 2 Top views of wind tunnel facility and blade details

Table 2 Details of turbulence grid and location

Grid	Location (s/d)	Turbulence Intensity
No Grid		0. 72%
Find Grid	60 cm (120)	3.1%
	30cm (60)	6%
	21cm (42)	8.2%
Coarse Grid	30cm (23)	13%

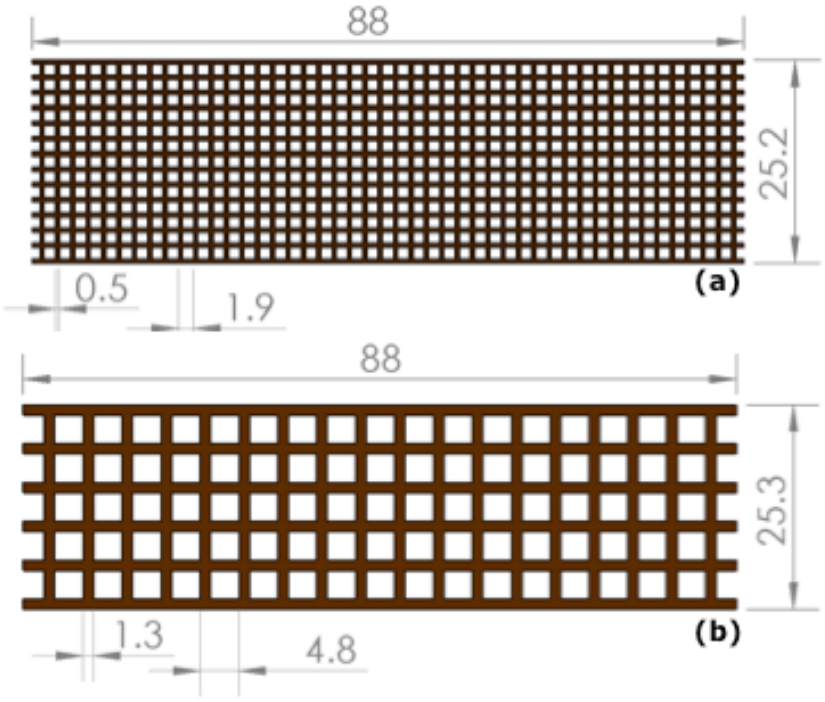

Figure 3 Turbulence grid (a) Fine grid. (b) Coarse grid

2.2 Platform Film Cooling Design

By the reason of difficulty to figure the real swirl ratio in a rotating turbine blade, assumptions were made that swirl ratio 0.4 is highly rotating condition with 60% of the relative motion, 0.6 is moderate rotating condition with 40% of the relative motion, and 1.0 is non-rotating condition with 0% of the relative motion. As the wind tunnel is stationary, velocity triangle analogy is used to simulate the relative motion between stator and rotor, which exists in real gas turbine engine. As seen in Figure 4, rotating condition in the real engine blade is brought to the stationary cascade, which makes the relative motion (Vr). The blue circle with arrows indicates the swirl motion of coolant (Vc). Each swirl ratio has a corresponding velocity ratios such as VR* and VR**. VR* is the ratio of circumferential velocity component to cascade inlet velocity, and VR** is the ratio of actual velocity to cascade inlet velocity, which are specified in Table 1. Figure 5 describes the process of the swirl purge/purge flow in the wind tunnel. Coolant was supplied from the plenum, and it passed through the coolant injection hole plate. After that, it touched the nozzle endwall and axisymmetric dolphin nose before entering to the blades. Axisymmetric dolphin nose contouring brought stream-wise acceleration and thin boundary layer due to steeper connection between slot cavity and blade leading edge, which reduced horseshoe vortex near leading edge. Figure 6 shows three different injection hole plates, which produced three kinds of swirl ratios motion. Coolant injection hole plates took the important role in this process because they implemented the swirl purge/purge flow motion from three different inclined angles. The inclined angle 45°and 60° made swirl purge flow with ratio 0.4, 0.6, and 90° made purge flow with

ratio1.0. On each plate, 50 cylindrical holes were distributed to eject uniform coolant. Each hole plate have different hole diameters and spacing, which were acquired from VR** in accordance with injection hole degree. Equation (1) and (2) explain the calculation procedures of hole diameters, and proves the validity of hole plate design. In the Equation (1), density ratio ρ_c / ρ_∞ is given as 1.5. In the Equation (2), MFR is given as 1.0, VR** is depending on injection degree, A_∞ is 0.2347 m^2 based on up stream cross section area of wind tunnel, and N is 50, so that D could be obtained according to each swirl ratio.

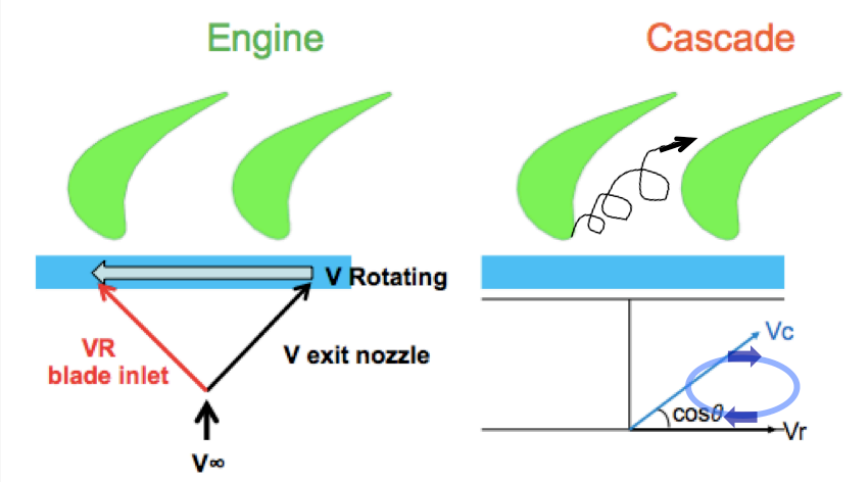

Figure 4 Velocity triangle analogy

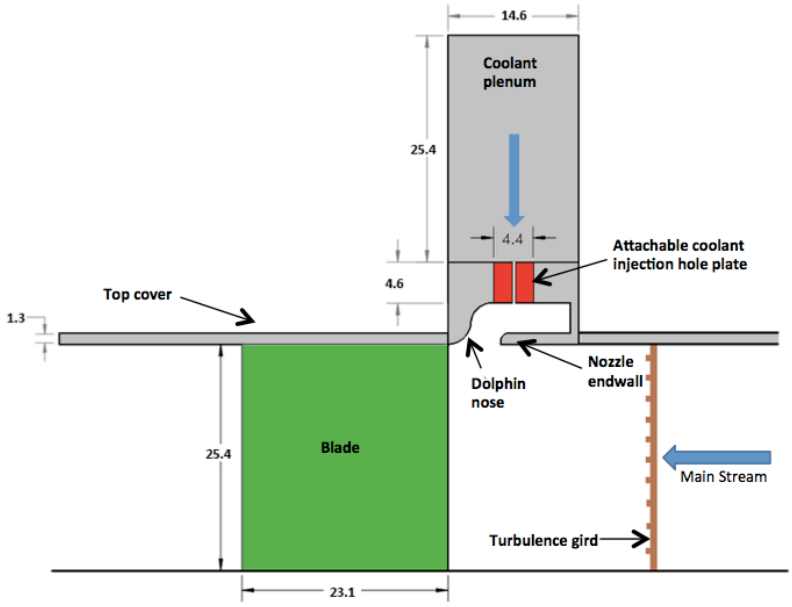

Figure 5 Side view of swirl purge flow design

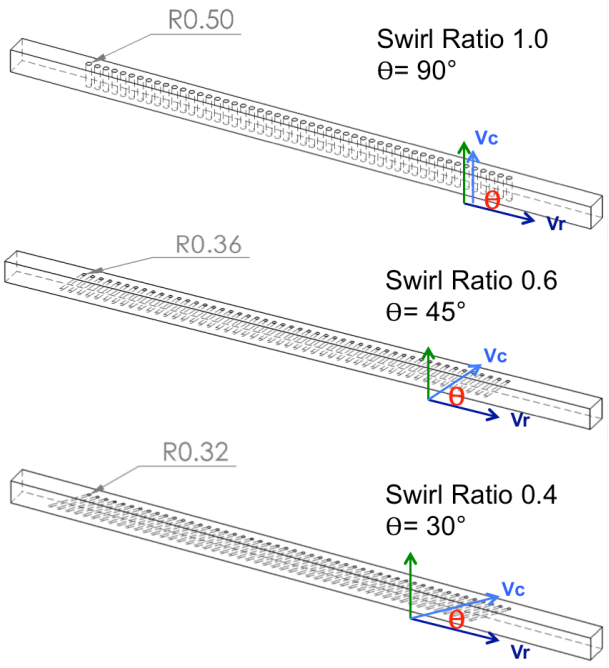

Figure 6 Coolant injection hole plates

$$\mathrm{MFR} = \frac{m_c}{m_\infty} = \frac{\rho_c}{\rho_\infty} \times \frac{V_c}{V_\infty} \times \frac{A_c}{A_\infty} = 1.5 \times \mathrm{VR} ** \times \frac{A_c}{A_\infty} \qquad \text{Equation (1)}$$

$$A_c = \frac{\mathrm{MFR} \times A_\infty}{1.5 \times \mathrm{VR}**} = \frac{\pi \times D^2 \times N}{4} \qquad \text{Equation (2)}$$

Figure 7 shows the detailed cooled passage that was painted with PSP. When coolant was injected, this region was taken by CCD camera that was installed in the bottom of the wind tunnel facility.

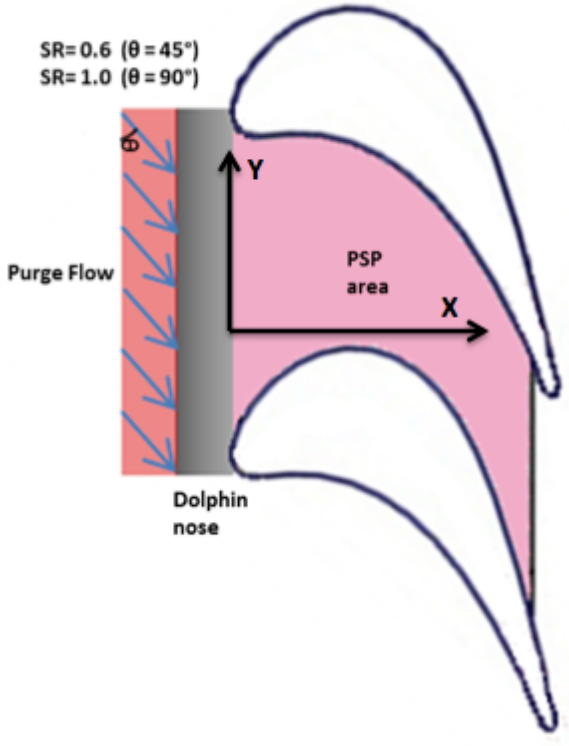

Figure 7 Detail of cooled passage

3. PRESSURE SENSITIVE PAINT METHOD

3.1 Measurement Theory

Pressure Sensitive Paint (PSP, UniFIB UF470-750 from ISSI Inc.) technique is based on the oxygen-quenched photoluminescence, so it provides not only detailed film cooling distribution but also it avoids false presentation from heat conduction. PSP is composed of photo-luminescent molecules that emit light with intensity proportional to the surrounding partial pressure of oxygen. When painted surface is excited by blue region with wavelength around 450nm, it emits light in the red region with higher wavelength around 600nm. A long pass filtered CCD camera (Cooke Sensicam) captures the light intensity. Since current study aims to achieve the quantitative details of film cooling effectiveness distribution on the platform PSP is appropriate for current study. The process of PSP is seen in Figure 8. McLachlan and Bell [44] explained the details of PSP working process. Han et al [45] introduced numerous thermal and fluid experimental methodologies and explained details of PSP procedure. They showed film cooling effectiveness distribution from various cooling source from gas turbine blade, which were acquired from PSP technique, it proved that PSP is powerful technique for the complicated geometry.

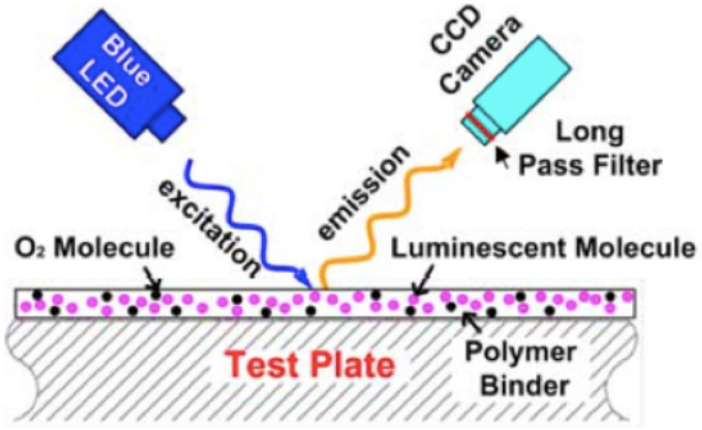

Figure 8 Process of PSP

3.2 PSP Calibration

A calibration performed to have a correlation between the light intensity (I) and partial pressure of oxygen surrounding the painted surface, which is written as Equation (3).

$$\frac{I_{ref}-I_{blk}}{I-I_{blk}} = f\left(\frac{P_{O_2}}{P_{O_2,ref}}\right) = f\left(P_{O_2}\right)$$
$$= K_0 + K_1(P_{ratio}) + K_2(P_{ratio})^2 + K_3(P_{ratio})^3$$
$$= -0.6048 + 1.1258\,(P_{ratio}) + 0.5115\,(P_{ratio})^2 - 0.0271\,(P_{ratio})^3$$

Equation (3)

I_{ref} is the reference intensity that is acquired at atmospheric condition to compensate for the non-uniformity of lighting. I_{blk} is the black intensity that is acquired in a dark room without mainstream to get rid of back ground noise. For calibration, a small Plexiglas block painted 7 coats of PSP were placed in the vacuum chamber, and

camera was on the top with various inclined angles from 20 to 90 degree to record the images through the optically clear window. The images were recorded at several pressures raging from 0~1.0 atm, and the emission intensities were recorded at each pressure. The intensities of each pressure and angles are well correlated as seen in the Figure 9.

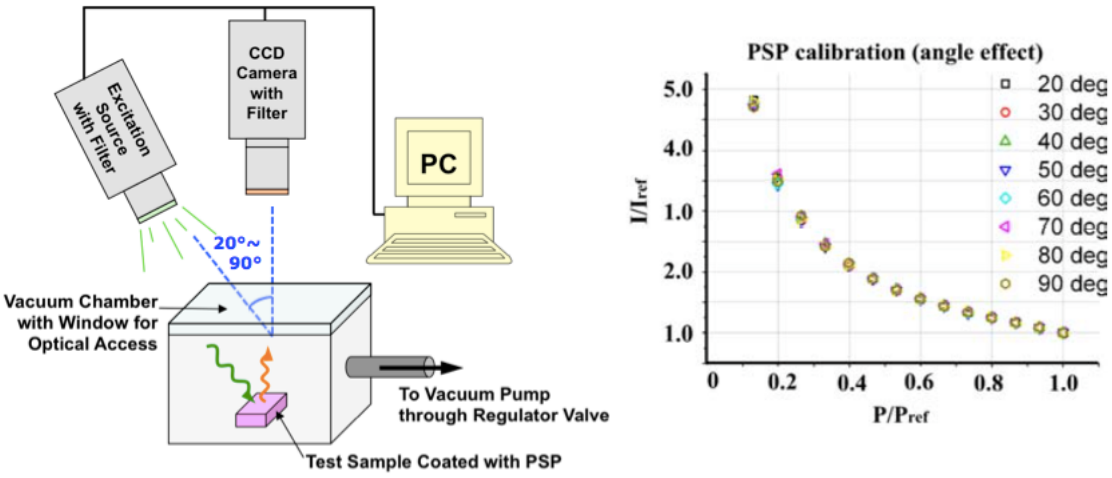

Figure 9 PSP calibrations

3.3 Film Cooling Effectiveness Calculation

To obtain one complete set of data, four different types of images were taken including reference and black image, and two different coolants are injected separately. One of the coolants was Air (same as mainstream) and the other is oxygen free foreign

gas. The tested wall was assumed adiabatic wall temperature, so the film cooling temperature was derived from a mass concentration (C) of oxygen, and the concentration (C) is expressed as a molecular weight (W) and partial pressure of oxygen (P_{O_2}) as seen by the equation (4). For current study, CO_2 was used to attain the density ratio 1.5, so the molecular ratio of the foreign gas to air ($\frac{W_{fg}}{W_{air}}$) is 1.5 in current study. The subscripts of f, m, c, aw, w and fg are film, mainstream, coolant, adiabatic wall, wall and foreign gas respectively.

$$\eta = \frac{\mathbf{T_f - T_m}}{\mathbf{T_c - T_m}} \approx \frac{\mathbf{T_{aw} - T_m}}{\mathbf{T_c - T_m}} \approx \frac{\mathbf{C_w - C_m}}{\mathbf{C_c - C_m}} = \frac{Co_2,fg - Co_2,air}{Co_2,c - Co_2,air}$$

$$= 1 - \frac{Co_2,fg}{Co_2,air} = 1 - \frac{1}{\left(\frac{(P_{O_2})_{air}}{(P_{O_2})_{fg}} - 1\right)\frac{W_{fg}}{W_{air}} + 1} \qquad \text{Equation (4)}$$

That is, due to the oxygen quenching process of PSP, the intensity (I) of tested surface is inversely proportional to the partial pressure of oxygen surrounding the surface. When foreign gas is injected, the oxygen mass concentration of coolant hole is zero, so higher intensity means less oxygen mass concentration and more coolant coverage on the surface.

3.4 Uncertainty Analysis

Three major uncertainties were estimated from Kline- McClintock technique. Mainstream velocity measurement had maximum 3% of error, which came from a micro-manometer in the upstream test section. Coolant mass flow rate measurement had

maximum 2% of error, which came from an orifice flow meter that was operated to supply the coolant. Film cooling effectiveness had maximum 3% of error, which came the uniformity of intensity of PSP illumination. That is, if the effectiveness were around 0.01, the actual effectiveness would be within the range of 0.0097~0.0103.

4. RESULTS AND DISCUSSION

4.1 Data Selection and Validity (Swirl Ratio 0.6 and all Tu cases)

Each test set was repeated for two to three times and repeated again in different days in order to have repeatability. Figure 10 shows the platform pitch wise averaged effectiveness from swirl ratio 0.6 with five turbulence intensities. The data that were obtained in a same day have a same line style (Solid or Dash) but different colors with trial order (Red, Blue and Black). The result from Tu = 0.72% is borrowed from the previous study [32].

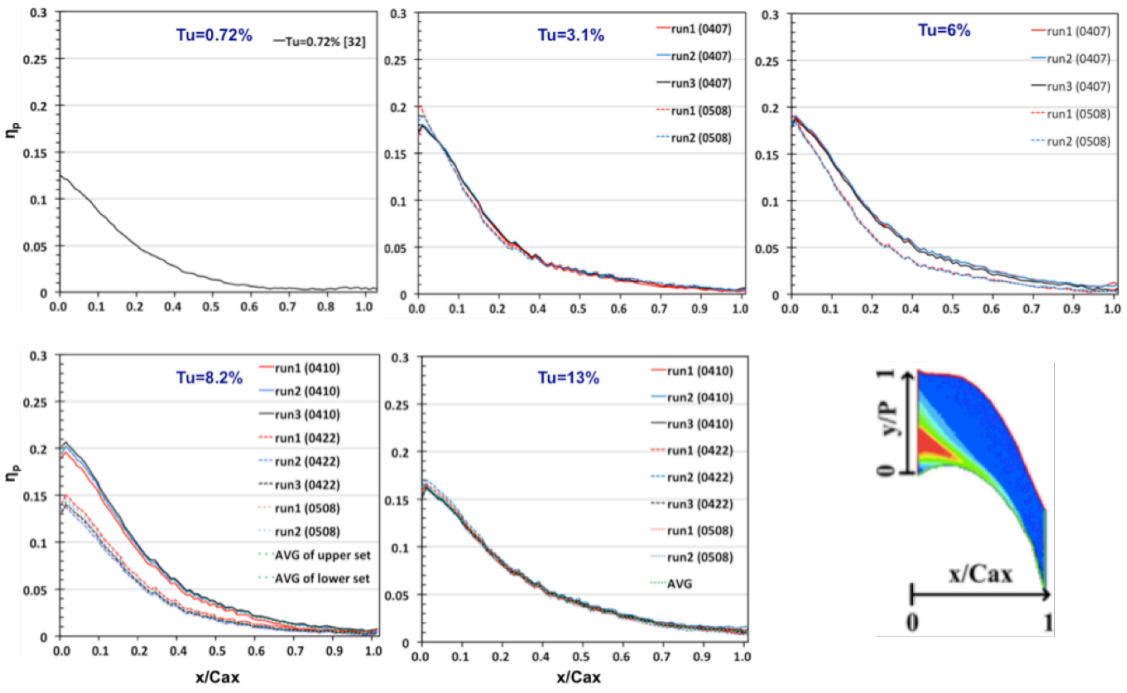

Figure 10 Whole test results of swirl ratio 0.6

The results of turbulence 3.1%, 6% and 8.2% have deviations between different data taking periods, specially Tu=8.2% has the most extreme deviation. For Tu=6% and 8.2%, the data that were taken in later periods (Dash line) have lower effectiveness than those were taken in earlier periods (Solid line)

Figure 11 shows the Tu effect comparison at given swirl ratios, which have two possible data sets A (upper) and B (Lower), and swirl ratio 0.4 and 1.0 are from previous study [43]. By the reason of data deviation between different data taking periods, two representative plots were selected for Tu= 3.1%, 6% and 8.2%. One plot was selected among earlier taking period data for set A, and the other plot was selected among later data taking period data for set B. Each representative plot for each turbulence case was the most coincident one with an average plot for the case. As a result, one reasonable set could be decided between set A and B by comparing the trend with swirl ratio 0.4 and 1.0.

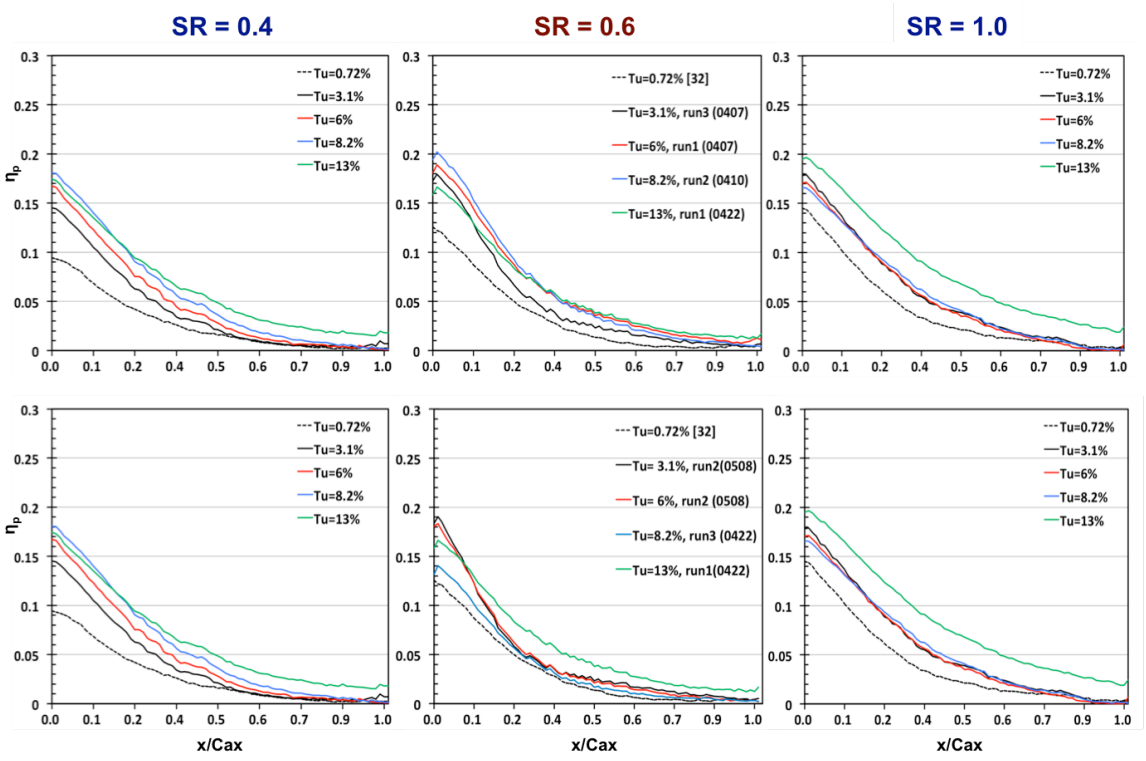

Figure 11 Quantitative comparisons of Tu effect

Overall, the film cooling effectiveness augmentation occurs when turbulence level increasing, and the augmentation level is significant when turbulence increased from Tu= 0.72% to 3.1% in all swirl ratios. Tu =13% has the highest film cooling effectiveness after the point of x/Cax=0.2 for swirl ratio 0.4. Tu =13% has the highest film cooling effectiveness significantly in all location for swirl ratio 1.0.

In case of swirl ratio 0.6 from set A, the film cooling effectiveness increasing with Tu increasing from 0.72% to 13%, and this case also has remarkable film cooling effectiveness augmentation when Tu increasing from 0.72% to 3.1%.

In case of swirl ratio 0.6 from set B, film cooling effectiveness increases significantly when Tu increasing from 0.72% to 3.1%, and Tu 3.1% and 6% have similar

trend. Film cooling effectiveness decreased for Tu=8.2% and large film cooling effectiveness augmentation occurs again for Tu=13%. When the film cooling effectiveness augmentation trend is compared with that of swirl ratio 0.4 and 1.0 cases, the earlier taken data set A has better validity.

Figure 12 shows the swirl ratio effect comparison at given Tu intensity. In the cases of swirl ratio 0.6 for Tu= 3.1%, 6% and 8.2%, each Tu case has two black lines; solid line is from earlier taken data and dash line is from later taken data. For the lowest Tu case (Tu=0.72%), swirl ratio effect is apparent that film cooling effectiveness decreasing with decreasing swirl ratio. This is because lower swirl ratio has larger tangential velocity component caused by higher relative motion between coolant and disk cavity, which enhances passage vortex and reduces coolant penetration capacity. As turbulence intensity further increasing, the plots of SR 0.4 and 1.0 (blue and red) get closer except for Tu=13% case. Under the consideration of this trend, the black solid lines (earlier taken data) have a better validity.

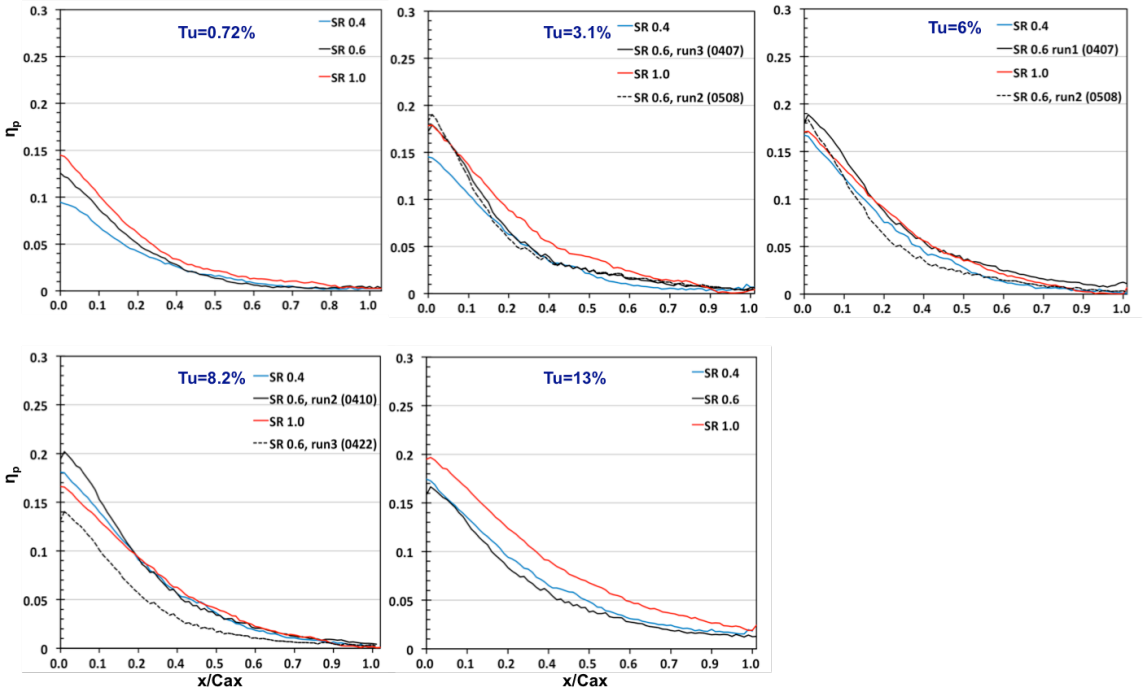

Figure 12 Quantitative comparison of swirl ratio effect

4.2 Final Results

Figure 13 and 14 indicate the final selected results from the data validation step. Figure 13 shows the effect of turbulence on blade platform with pitch wise averaged film cooling effectiveness along x direction. Higher Tu improves the film cooling effectiveness, especially; Tu increasing from 0.72% to 3.1 % leads remarkable effectiveness increment. After that, effectiveness increases slightly for further Tu increasing from 3.1% to 13% under rotating condition. However, there is almost no Tu effect when Tu increasing from 3.1% to 8.2% under non-rotating condition. In general, Tu 13% has the higher effectiveness throughout the blade passage, and Tu 13% has the outstanding effectiveness under non- rotating condition.

Figure 14 shows the effect of swirl ratio for each turbulence intensities. Swirl ratio effect is obvious for low Tu cases (Tu=0.72% and 3.1%), however, those three lines get closer to each other, swirl ratio effect is declined, as Tu increasing.

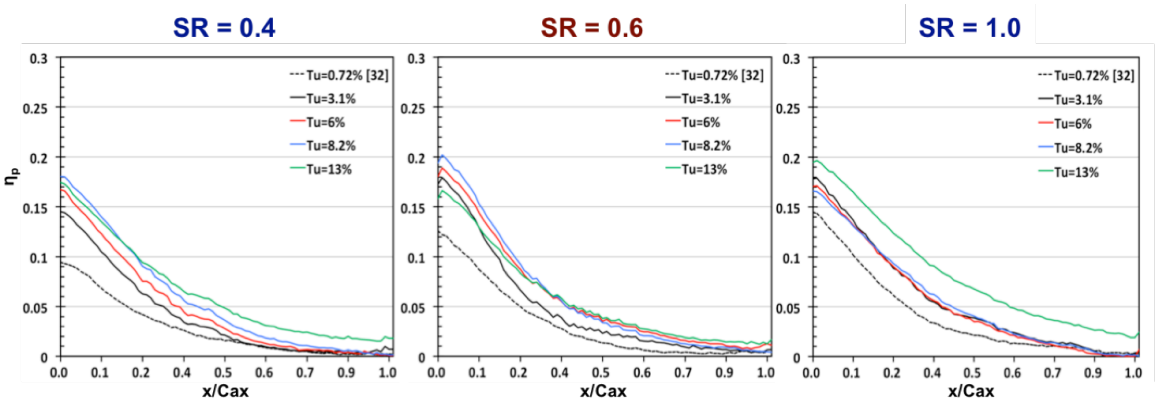

Figure 13 Final results of Tu effect

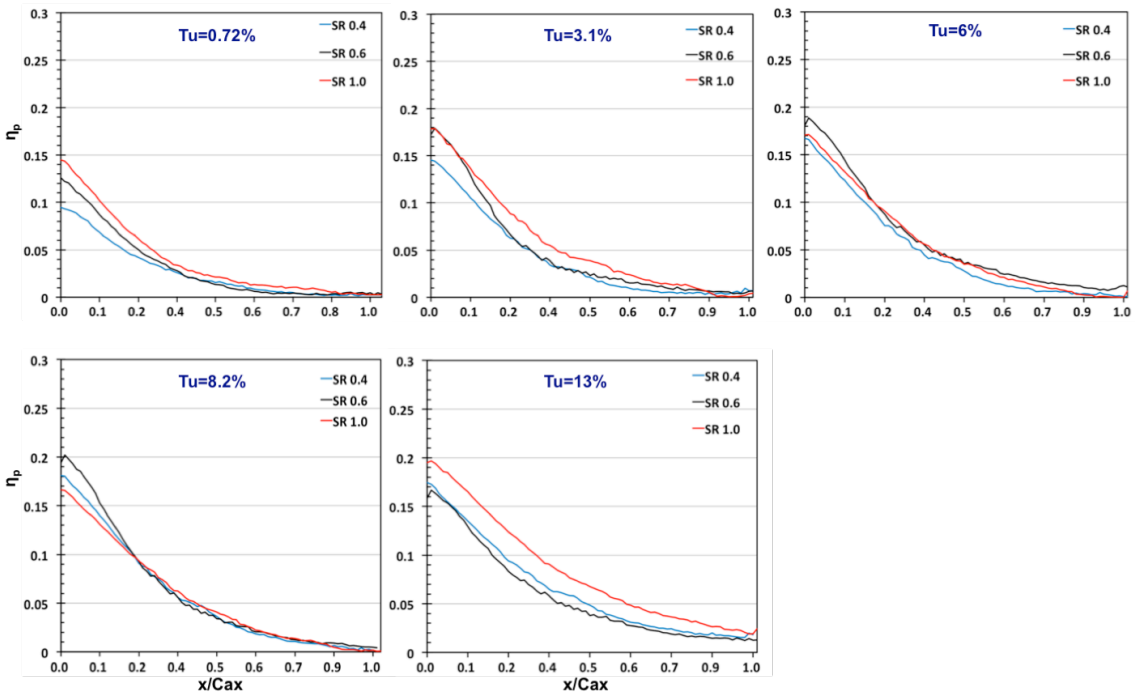

Figure 14 Final result of swirl ratio effect

4.3 Film Cooling Effectiveness Distribution on Platform

Figure 15. shows the film cooling effectiveness distribution on the platform. Overall, coolant is toward to suction side as the coolant travels to the trailing edge. A horseshow vortex forms at the junction between blade leading edge and platform. The vortex separates into pressure side and suction side legs. Suction side leg continuously moves along the suction surface, and pressure side leg develops and merges with passage vortex. When the flow turns, a pressure gradient occurs between pressure side and suction side, which result in passage vortex moving to suction side. The coolant is swept by this strong passage vortex and turns to the suction side, which makes uncooled area in pressure side.

Mainstream turbulence expands the platform cooling coverage as the turbulence intensity increasing for all swirl ratios, especially increment level of film cooling is highest when turbulence increased from 0.72% to 3.1%. Turbulence makes the thinner boundary layer in upstream and reduces the strength of horseshoe vortex. Also, turbulence is able to break down the passage vortex in lateral region, which leads more uniform coolant distribution. The highest turbulence intensity (13%) has the most uniform and widest coolant distribution.

Swirl ratio effect is apparent as seen in the Figure 15 by comparing the upper (Swirl ratio =0.4) and lower (Swirl ratio =1.0) sub-figures. Swirl ratio 0.4 case; the highest relative motion case, has lower film cooling effectiveness for a given turbulence intensity because it has the largest tangential velocity component of swirl purge flow, which induces stronger rotation vortex. Strong passage vortex makes the coolant life off from the platform rather than touch it. On the other hand, swirl ratio 1.0 case; non-rotating and no relative motion case, has the most effective cooling. The reason why the coolant is still toward to suction side in SR 1.0 is due to pressure gradient existence even in non-rotating condition. Consequently, swirl effect brings the negative result to cooling coverage.

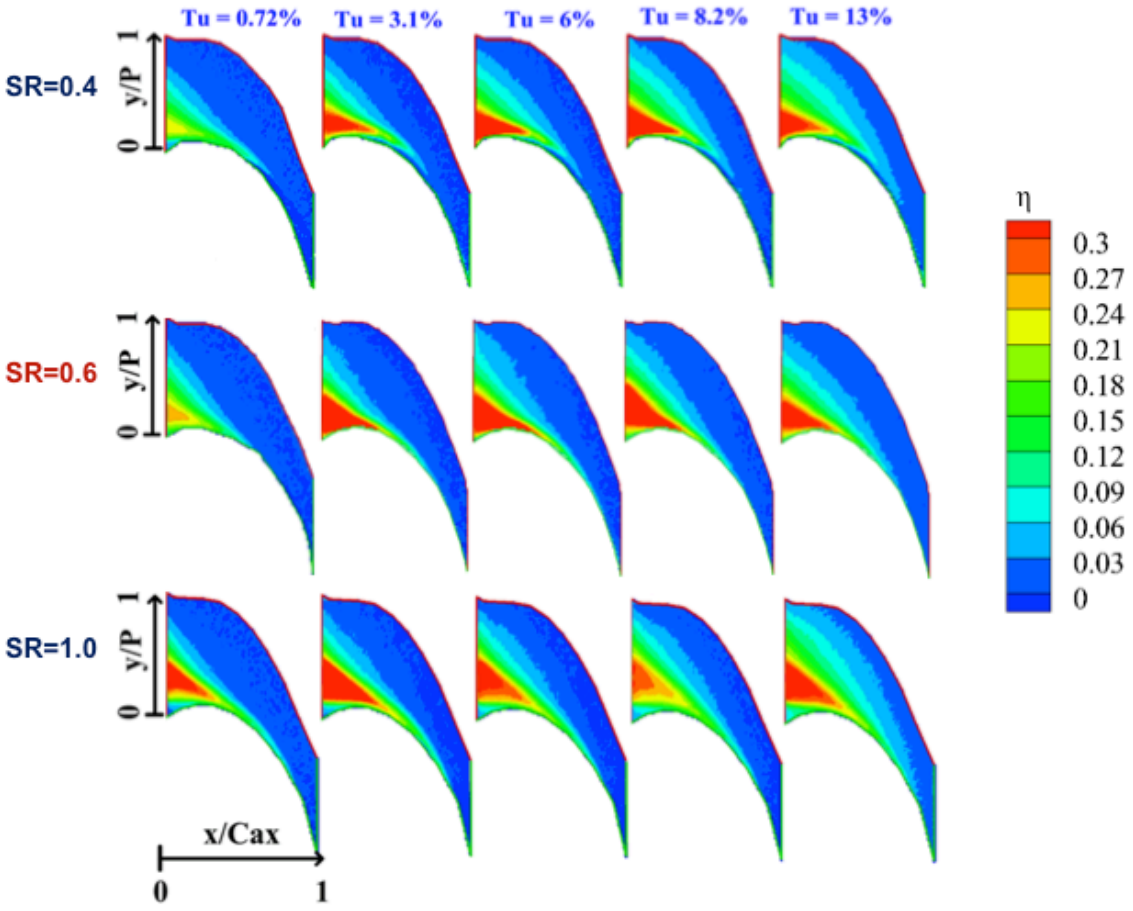

Figure 15 Contours of film cooling on blade platform

5. CONCLUSIONS

An experimental study was performed to measure the effect of mainstream turbulence ranges from 0.72% to 13% and the effect of swirl purge flow on blade platform. Advanced inclined injection hole design and endwall trailing edge were equipped to simulate the relative motion between stator and rotor that exists in rotating turbine. Main conclusions are below.

5.1 Coolant Distribution

Two main secondary flow; horseshoe vortex and passage vortex, were shown apparently because of pressure gradient between suction side and pressure side. They dominate the overall coolant movement and make the coolant toward to suction side as it travels to downstream. Therefore, pressure side region has poor film cooling coverage.

5.2 Mainstream Turbulence Effect

Higher mainstream turbulence improves the purge flow cooling effectiveness because turbulence makes thinner boundary layer, which reduce horseshoe vortex near leading edge area, and turbulence breaks down the passage vortex in the lateral region. That is, turbulence is able to weaken the vortex. This positive effect is significant when turbulence increases from 0.72% to 3.1% in all swirl ratio cases. Turbulence 13% case has generally highest effectiveness throughout the platform.

5.3 Swirl Ratio Effect

Overall, swirl purge flow cases (SR 0.4 and 0.6) have less film cooling effectiveness than the purge flow case (SR 1.0). Rotating condition enhanced the tangential velocity component of purge coolant and swirl motion, which results in less axial penetration of purge coolant

Swirl purge flow induces stronger passage vortex, which causes poor cooling performance on blade platform. On the other hand, mainstream turbulence is positive, but it is still not enough to cover the whole passage. To compensate the uncooled region, additional cooling sources, such as discrete film-cooling holes, should be utilized. This study is valuable in terms of demonstrating the combination effect of swirl purge flow and mainstream turbulence effect.

REFERENCES

[1] Han, J. C., 2013, "Fundamental Gas Turbine Heat Transfer," Journal of Thermal Science and Engineering Applications, Vol. 5(2), pp. 021007.

[2] Langston, L., 1980, "Cross Flow in Turbine Cascade Passage," Journal of Engineering for Power, Vol. 102(1), pp. 866-874.

[3] Langston, L., 2001, "Secondary Flows in Axial Turbines – A Review," Annals of the New York Academy of Sciences, Vol. 934(1), pp. 11-26.

[4] Wang, H., Olson, S., Goldstein, R., and Eckert, E., 1995, "Flow Visualization in a Linear Turbine Cascade of High Performance Turbine Blades," ASME 1995 International Gas Turbine and Aero engine Congress and Exposition, Paper No. 95-GT-007

[5] L. M. Wright, M. F. Malak, D. C. Crites, M. C. Morris, V. Yelavkar, and R. Bilwani., 2014 “Review of Platform Cooling Technology for High Pressure Turbine Blades,” Proceedings of ASME Turbo-Expo 2014, Paper No. GT2014-26373.

[6] Harasgama, S. P., and Burton, C. D., 1992, “Film Cooling Research on the Endwall of a Turbine Nozzle Guide Vane in a Short Duration Cascade Part 1: Experimental Technique and Results,” Journal of Turbomachinery, Vol. 114.4, pp. 734-740.

[7] Friedrichs, S., Hodson, H. P., and Dawes, W. N., 1995, “Distribution of Film Cooling Effectiveness on a Turbine Endwall Measured Using the Ammonia and Diazo Technique,” ASME 1995 International Gas Turbine and Aeroengine Congress and Exposition, Paper No. 95-GT-001

[8] Jabbari, M. Y., Marston, K. C., Echert, E. R. G., and Goldstein, R. J., 1994, “Film Cooling of the Gas Turbine Endwall by Discrete-Hole Injection,” ASME 1994 International Gas Turbine and Aeroengine Congress and Exposition, Paper No. 94-GT-067

[9] Liu, S., Liu, G., Xu, D., Lapworth, B. L., and Forest, A. E., 1999, “Aerodynamic Investigation of Endwall Film-Cooling in an Axial Turbine Cascade Part I: Experimental Investigation,” AIAA ISABE Symposium on Air Breathing Engines, Paper No. ISABE 99-7080.

[10] Granser, D., and Schulenberg, T., 1990, “Prediction and Measurement of Film cooling Effectiveness for a First-Stage Turbine Vane Shroud,” ASME 1990 International Gas Turbine and Aeroengine Congress and Exposition, Paper No. 90-GT-095

[11] Roy, R., Squires, K., Gerendas, M., Song, S., Howe, W., and Ansari, A., 2000, "Flow and Heat Transfer at the Hub Endwall of Inlet Vane Passages - Experiments and Simulations," ASME Turbo Expo 2000: Power for Land, Sea, and Air, Paper No. 2000-GT-198.

[12] Lapworth, B. L., Forest, A. E., and Liu, S., 1999, “Aerodynamic Investigation of Endwall Film-Cooling in an Axial Turbine Cascade Part II: Numerical Investigation,” AIAA ISABE Symposium on Air Breathing Engines, Paper No. ISABE 99-7193.

[13] Oke, R. A., and Simon, T. W., 2002, “Film Cooling Experiments with Flow Introduced Upstream of a First Stage Nozzle Guide Vane Through Slots of Various Geometry,” ASME Turbo Expo 2002: Power for Land, Sea, and Air, Paper No. GT-2002-30169.

[14] Colban, W. F., Thole, K. A., and Zess, G., 2002, “Combustor Turbine Interface Studies – Part 1: Endwall Effectiveness Measurements,” ASME Turbo Expo 2002: Power for Land, Sea, and Air, Paper No. GT-2002-30526.

[15] Kost, F., and Nicklas, M., 2001, “Film-Cooled Turbine Endwall in a Transonic Flow Field: Part I- Aerodynamic Measurements,” Journal of Turbomachinery, Vol. 123, pp. 709-719.

[16] Nicklas, M., 2001, “Film-Cooled Turbine Endwall in a Transonic Flow Field: Part II- Heat Transfer and Film-Cooling Effectiveness,” Journal of Turbomachinery, Vol. 123, pp. 720-729.

[17] Zhang, L. J., and Jaiswal, R. S., 2001, “Turbine Nozzle Endwall Film Cooling Study Using Pressure-Sensitive Paint,” Journal of Turbomachinery, Vol. 123, pp. 730-738.

[18] Zhang, L. J., and Moon, H. K. 2003, “Turbine Nozzle Endwall Inlet Film Cooling – the Effect of a Back-Facing Step,” ASME Turbo Expo 2003, collocated with the 2003 International Joint Power Generation Conference, Paper No. GT-2003-38319.

[19] Zhang, L. J., and Moon, H. K., 2004, “Turbine Nozzle Endwall Inlet Film Cooling – the Effect of a Back-Facing Step and Velocity Ratio,” ASME International Mechanical Engineering Congress and Exposition 2014, Paper No. IMECE2004-59117.

[20] Zhang, L. J., and Moon, H. K. 2011, “Comparison of Two Axisymmetric Profiles on Blade Platform Film Cooling,” ASME 2011 Turbo Expo: Turbine Technical Conference and Exposition, Paper No. GT2011-45102.

[21] Burd, S. W., and Simon, T. W., 2000, “Effects of Slot Bleed Injection over a Contoured Endwall on Nozzle Guide Vane Cooling Performance: Part I – Flow Field Measurements,” ASME Turbo-Expo 2000: Power for Land, Sea, and Air, Paper No. 2000-GT-199.

[22] Burd, S. W., Satterness, C. J., and Simon, T. W., 2000, “Effects of Slot Bleed Injection over a Contoured Endwall on Nozzle Guide Vane Cooling Performance: Part II – Thermal Measurements,” ASME Turbo-Expo 2000: Power for Land, Sea, and Air, Paper No. 2000-GT-200.

[23] Oke, R. A., Burd, S. W., Simon, T. W., and Vahlberg, R., 2000, “Measurements in a Turbine Cascade over a Contoured Endwall: Discrete Hole Injection of Bleed Flow,” ASME Turbo- Expo 2000: Power for Land, Sea, and Air, Paper No. 2000-GT-214.

[24] Zhang, L. J. Dong H. Lee, Juan Yin and Moon, H. K., 2013, “The Effect of Axisymmetric Profile on Turbine Blade Platform Heat transfer Distribution,” Proceeding of ASME Turbo-Expo 2013, Paper No. GT2013-94335.

[25] Gao, Z., Narzary, D., Mhetras, S., and Han, J. C., 2009,"Turbine Blade Platform

Film Cooling with Typical Stator –Rotor Purge Flow and Discrete-Hole Film Cooling," Journal of Turbomachinery, 131, pp. 041004

[26] Wright, L. M., Blake, S. A., Rhee, D. H., and Han, J. C., 2009, "Effect of Upstream Wake with Vortex on Turbine Blade Platform Film Cooling with Simulated Stator-Rotor Purge Flow," Journal of Turbomachinery, Vol. 131, pp. 021017.

[27] Wright, L.M., Blake, S., and Han, J.C., 2008, "Film Cooling Effectiveness Distribution on a Gas Turbine Cascade Platform with Stator-Rotor Purge and Discrete Film-Hole Flows," Journal of Turbomachinery, Vol. 130, pp. 031015.

[28] Suryanarayanan, A., Mhetras, S., Schobeiri, M., and Han, J. C., 2009, "Film-Cooling Effectiveness on a Rotating Blade Platform" Journal of Turbomachinery, Vol. 131(1), pp. 011014.

[29] Rezasoltani, M., Schobeiri, M. T., and Han, J. C., 2013,"Experimental Investigation of the Effect of Purge Flow on Film Cooling Effectiveness on a Rotating Turbine with Non-Axisymmetric Endwall Contouring," Proceeding of ASME Turbo-Expo 2013, San Antonio, Texas, June 3-7, Paper No. GT2013-94807

[30] Barigozzi, G., Franchini G., Perdichizzi, A., Maritano, M., and Abram, R., 2013, "Influence of Purge Flow Injection Angle on the Aero-Thermal Performance of a Rotor Blade Cascade," Proceeding of ASME Turbo-Expo 2013, San Antonio, Texas, June 3-7, Paper No.GT2013-94692.

[31] Stinson Matthew, Goldstein, R. J., Simon, T.W., Fujimoto Shu, and Nakamata Chiyuki, 2014, "Effect of Swirled Leakage Flow on Endwall Film Cooling," Proceeding of the 15th International Heat Transfer Conference, Kyoto, Japan, August 10-15, Paper No. IHTC 15-9600.

[32] Li, S. J., Lee. J., Han. J. C., Zhang. L., and Moon. H. K., Turbine Platform Cooling and Blade Surface Phantom Cooling from Simulated Swirl Purge Flow, Proceedings of ASME Turbo-Expo 2015, Montreal, Canada, 2015, Paper No. GT2015-42263.

[33] Jumper, G. W., Elrod, W. C., and Rivir, R. B., 1991, “Film cooling Effectiveness in High Turbulence Flow,’’ Journal of Turbomachinery, Vol. 113, pp. 479–483.

[34] Radomsky, R. W., and Thole, K. A., 2000, “High Free-Stream Turbulence Effects on Endwall Heat Transfer for a Gas Turbine Stator Vane,” Journal of Turbomachinery, Vol.122, pp. 299–708.

[35] Radomsky, R,W., and Thole, K. A., “Flow field Measurements for a Highly Turbulence Flow in a Stator Vane Passage” Journal of Turbomachinery, Vol. 122(2), pp. 255-262.

[36] L. Zhang, and J. C. Han, 1994, “Influence of Mainstream Turbulence on Heat Transfer Coefficients From a Gas Turbine Blade” Journal of Heat Transfer, Vol. 116, pp. 896-903.

[37] Liu, K., Yang, S.F., and Han, J. C., 2013, “Influence of Coolant Density on Turbine Platform Film-Cooling with Stator-Rotor Purge Flow and Compound-Angle Holes,” Proceeding of ASME Turbo-Expo 2013, San Antonio, Texas, June 3-7, Paper No. GT2013-94155.

[38] Kadotani, K., and Goldstein, R., 1979, "On the Nature of Jets Entering a Turbulent Flow Part A: Jet-Mainstream Interaction," Journal of Engineering for Journal of Engineering for Gas Turbines and Power, Vol. 101, pp. 459- 465.

[39] Kadotani, K., and Goldstein, R., 1979, "On the Nature of Jets Entering a Turbulent Flow Part B: Film Cooling Performance," Journal of Engineering for Gas Turbines and Power, Vol. 101.3, pp 466-470.

[40] Bons, J. P., MacArthur, C. D., and River, R. B., 1996, "The Effect of High Free-Stream Turbulence on Film Cooling Effectiveness," Journal of Turbomachinery, Vol. 118(4), pp. 814- 825.

[41] Gregory-Smith, D. G., and Cleak, J. G. E., 1992, ‘‘Secondary Flow Measurements in a Turbine Cascade With High Inlet Turbulence,’’ Journal of Turbomachinery, Vol.

110, pp. 1–8.

[42] F. E. Ames, P. A. Barbot, and C. Wang, 2003, “Effects of Aero derivative Combustor Turbulence on Endwall Heat Transfer Distributions Acquired in a Linear Vane Cascade,” Journal of Turbomachinery, Vol. 125, pp. 210-220.

[43] Li, S. J., Lee. J., Han. J. C., Zhang. L., and Moon. H. K., "Influence of Mainstream Turbulence on Turbine Blade Platform Cooling from Simulated Swirl Purge flow” ASME-ATI-UIT 2015 Thermal energy system, Napoli, Italy.

[44] McLachlan, B., and Bell, J., 1995, "Pressure-Sensitive Paint in Aerodynamic Testing," Experimental Thermal and Fluid Science, Vol. **10**(4), pp. 470-485.

[45] Han, Je-Chin, and Akhilesh P. Rallabandi., 2010, "Turbine Blade Film Cooling Using PSP Technique." Frontiers in Heat and Mass Transfer, Vol.1(1), pp. 301